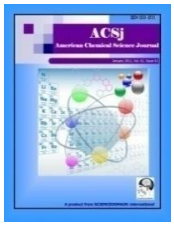

American Chemical Science Journal
6(3): 144-157, 2015, Article no.ACSj.2015.046
ISSN: 2249-0205

SCIENCEDOMAIN *international*
www.sciencedomain.org

New Properties and Characteristics of Mixed Ligand Coordination Polymers Derived from Transition Metal Ions, 1,2,4,5-Benzenetetracarboxylate and Aromatic Diamines

Aref A. M. Aly[1*], Asma I. El-Said[1], R. Gabr[1] and Rasel. A. Mukred[2]

[1]Department of Chemistry, Faculty of Science, Assiut University, Egypt.
[2]Department of Chemistry, Faculty of Education, Al-Baida University, Yemen.

Authors' contributions

This work was carried out in collaboration between all authors. Author AAMA designed in part the study, wrote the protocol, and wrote the first draft of the manuscript. Authors AIES and RG designed in part the study and managed the data analyses of the study. Author RAM managed the literature searches and performed the practical study. All authors read and approved the final manuscript.

Article Information

DOI: 10.9734/ACSj/2015/15754
Editor(s):
(1) Hsing-Lin Wang, Chemistry Division, Los Alamos National Laboratory, USA.
Reviewers:
(1) Anonymous, Serbia.
(2) Olga Kovalchukova, Department of General Chemistry, Peoples' Friendship University of Russia, Russia.
(3) Anonymous, Egypt.
(4) Anonymous, Serbia.
Complete Peer review History: http://www.sciencedomain.org/review-history.php?iid=901&id=16&aid=8348

Original Research Article

Received 16th December 2014
Accepted 19th February 2015
Published 4th March 2015

ABSTRACT

Coordination polymers derived from 1,2,4,5-benzenetetracarboxylate (H_2btec^{2-} or $btec^{4-}$), Fe(**II**), Mn(**II**), Co(**II**), Ni(**II**), Cu(**II**), Cd(**II**) or UO_2(**II**) metal ions, 1,10-phenanthroline(1,10-phen) or 2,2'-bipyridine(2,2'-bipy) were prepared. The polymers were characterized by elemental analysis, IR and electronic spectra, electrical conductance, magnetic susceptibility measurements and thermal behavior. The electronic spectra, magnetic susceptibility measurements and X-ray structure determination revealed octahedral and tetrahedral geometries around the metal ions. Kinetic and thermodynamic parameters of the thermal decomposition were computed from the thermal data using the Coats-Redfern equation. From the X-ray powder diffraction the particle sizes (6.4-25.4 nm) of the coordination polymers could be calculated using the Scherrer's equation.

**Corresponding author: E-mail: aref_20002001@yahoo.com;*

Keywords: Coordination polymers; spectra; thermal analysis.

1. INTRODUCTION

Coordination polymeric networks have been a field of rapid growth due to their intriguing variety of architectures and topologies as well as their special physical properties and potential application in many functional materials [1,2]. The coordination chemistry of aromatic polycarboxylate metal complexes has received considerable attention owing to the variety of bridging abilities of polycarboxylates in the formation of coordination polymers of different coordination modes [3,4]. 1,2,4,5-Benzenetetracarboxylic acid (H_4btec) possesses several interesting characteristics: (a) it contains four carboxyl groups which are subjected to be completely or only partially deprotonated, thus leading to interesting structures with higher dimensions and (b) the acid can act as a hydrogen-bond acceptor as well as hydrogen bond donor, according to the number of the deprotonated carboxyl groups. Hence, H_4btec is a good candidate for the construction of coordination polymers of different motifs. Mixed ligand coordination polymers with transition and non-transition metals incorporating 1,2,4,5-benzenetetracarboxylate, 1,10-o-phenanthroline or 2,2`-bipyridine were reported in the literature [5a-5c]. However, these coordination polymers lack detailed thermogravimetric analysis and biological screening. We embarked, therefore on the preparation of a series of coordination polymers comprising the ligands illustrated in Fig. 1 using preparation procedures differing from those reported earlier, which gave coordination polymers containing variable coordinated water or water of crystallization.

2. EXPERIMENTAL

All chemicals were of analytical grade. 1,2,4,5-Benzenetetracarboxylic acid (H_4btec) and 2,2'-bipyridine were purchased as E. Merck grade. 1,10-Phenanthroline was a Fluka grade. They were used without further purification.

2.1 Preparation of the Complexes

The compounds were prepared by mixing different molar ratios of the neutralized 1,2,4,5-benzenetetracarboxylic acid (H_4btec),o-phenanthroline (phen) or 2,2'-bipyridine (2,2'-bipy) and the metal ions in aqueous methanolic solutions under continuous stirring for 2 h. The precipitated complexes were filtered off and washed with ethanol and dried in a desiccator over P_2O_5.

2.2 Physical Measurements

Stoichiometric analysis (C, H, N, S) was performed using Analyischer Funktionstest Vario El Fab-Nr.11982027 elemental analyzer. The I.R spectra were recorded on a Shimadzu IR-470 spectrophotometer and the electronic spectra were obtained using a Shimadzu UV-2101 PC spectrophotometer. The thermal studies were carried out on a Shimadzu corporation 60H thermogravimetric analyses at a heating rate of 10ºC min^{-1}. Magnetic moments were measured at room temperature using magnetic susceptibility balance of type MSB-Auto. Molar susceptibilities were corrected for diamagnetism of the component atoms by the use of the Pascal's constants. The calibrant used was $Hg[Co(SCN)_4]$. The x-ray powder diffractometer was a Philips 1700 version with H. TPw 1370/10, 4 KVA CuKαλ=1.54180 Á. The conductivity of the complexes (10^{-3}M solutions) was measured using a conductivity meter model 4310 JENWAY.

2.3 Antimicrobial Activity Test

In vitro antimicrobial activities of two of the complexes were tested against a number of bacteria and fungi using the paper disc diffusion method [6].The nutrient agar and nutrient broth media were autoclaved for 20 min. at 121°C and 15 1b pressure before inoculation. Then a suspension of the bacterial or fungal strains in nutrient broth medium was prepared after cooling in a test tube. From that suspension 0.3 ml were taken in petri dishes where the nutrient agar was poured onto the plate and the petri dishes were shaked well and allowed to solidify. The test complexes dissolved in DMF were added drop wise to a 6 mm diameter filter paper disc placed at the center of each agar plate. The plates were then kept in an incubator at 37ºC. The width of the growth inhibition zone around the disc was measured after 24 h incubation.

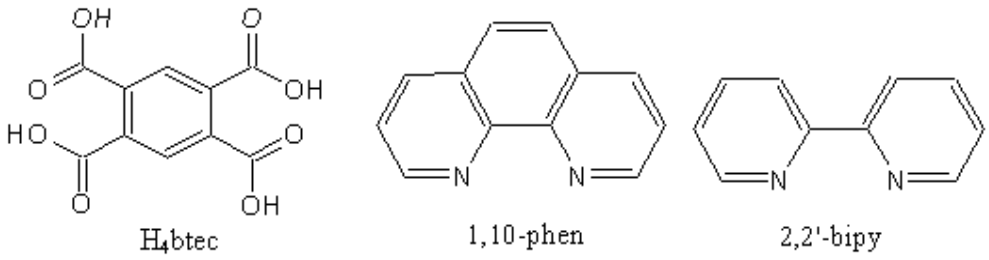

Fig. 1. Structure of the primary and secondary ligands

3. RESULTS AND DISCUSSION

Preparation of the complexes proceeds according to the following equations 1-5

$$2MCl_2.2H_2O+H_4btec+4NaOH+2diamine \xrightarrow[medium]{aq./methanolic} \{[M_2(btec)(diamine)_2(H_2O)_2].H_2O\}_n+ 4NaCl \quad (1)$$

where M= Mn(II) or Cu(II), diamine=1,10-phenanthroline or 2,2'-bipyridine

$$2FeCl_3.6H_2O+2H_4btec+6NaOH+2diamine \xrightarrow[medium]{aq./methanolic} \{[Fe_2(btec)(H_2btec)(diamine)_2(H_2O)_2].xH_2O\}_n+6NaCl \quad (2)$$

where x = 4 or 8.

$$2MCl_2.6H_2O+H_4btec+4NaOH+2phen \xrightarrow[medium]{aq./methanolic} \{[M_2(btec)(phen)_2(H_2O)_2].xH_2O\}_n+ 4NaCl \quad (3)$$

where M= Co(II) or Ni(II), x = 8or 6.

$$2Cd(NO_3)_2.4H_2O+H_4btec+4NaOH+2diamine \xrightarrow[medium]{aq./methanolic} \{[Cd_2(btec)(diamine)_2(H_2O)_2]2H_2O\}_n+4NaNO_3 \quad (4)$$

$$2UO_2(CH_3COO)_2.2H_2O+H_4btec+4NaOH+2diamine \xrightarrow[medium]{aq./methanole} \{[(UO_2)_2(btec)(diamine)_2]xH_2O\}_n+4CH_3COONa \quad (5)$$

where x = 4 or 2.

The conductivity was measured using 10^{-3} M in DMSO solutions. From Table 1 it could be concluded that all complexes are non-conductive as indicated by the low molar conductivity values varied in the range 22-56 $Ω^{-1}cm^2$ mol^{-1}.

3.1 IR Spectra

The main absorption peaks in the infrared spectra of the complexes are listed in Table 2 and Fig. 2. The absence of any bands around 1720 cm^{-1} for complexes **1, 4, 5, 6,7, 8, 9**, **10** and **11** indicates that all carboxylic groups are deprotonated. For the two iron(III) complexes **2** and **3**, the protonated and deprotonated carboxylates are involved in coordination. The two complexes display for the free carboxylate group a band at 1700 and 1690 cm^{-1}, respectively. All the coordination polymers exhibit a band in the regions1580-1530 and 1415-1365 cm^{-1} indicating coordination of the unprotonated carboxlate groups [7] and corresponding to their asymmetric and symmetric stretching vibration. The Δν difference (asymmetric–symmetric) in the complexes **(1-9)** occurs in the range 150-200 cm^{-1}, and the value proved that the carboxylate group is coordinated to the metal ions in a monodentate fashion [8,9]. In complexes **10** and **11** the carboxylates are bonded in the bidentate mode as the Δν lies in the range 210-215 cm^{-1} for both complexes. All complexes exhibit a band in the range 3300 -3500 cm^{-1} attributed to the lattice water molecules [10], whereas the stretching vibration of the coordinated water

Table 1. Color, molar conductance, elemental analysis and melting points of the complexes

Complex		Color	Λm ($Ω^{-1}cm^2$ mol^{-1})	Found (Calcd.%)			M.p., ºC (Decomp.)
				C	H	N	
$\{[Mn_2(btec)(phen)_2(H_2O)_2].H_2O\}_n$	**1**	Gray	30	51.08 (52.73)	3.00 (3.12)	5.99 (7.23)	>360
$\{[Fe_2(btec)(H_2btec)(phen)_2(H_2O)_2].4H_2O\}_n$	**2**	Dark-brown	25	47.11 (48.82)	3.72 (3.16)	4.50 (5.17)	296
$\{[Fe_2(btec)(H_2btec)(2,2'\text{-bipy})_2(H_2O)_2].8H_2O\}_n$	**3**	Dark-brown	45	42.10 (43.42)	3.70 (3.82)	4.30 (5.06)	300
$\{[Co_2(btec)(phen)_2(H_2O)_2].8H_2O\}_n$	**4**	Pink	26	43.50 (44.95)	4.10 (4.21)	5.13 (6.16)	>360
$\{[Ni_2(btec)(phen)_2(H_2O)_2].6H_2O\}_n$	**5**	Sky-blue	22	45.30 (46.83)	3.80 (3.92)	5.00 (6.42)	>360
$\{[Cu_2(btec)(phen)_2(H_2O)_2].H_2O\}_n$	**6**	Light -blue	43	51.52 (51.58)	4.30 (3.05)	5.8 (7.07)	260
$\{[Cu_2(btec)(2,2'\text{-bipy})_2].H_2O\}_n$	**7**	Dark -blue	45	48.48 (50.92)	3.08 (2.85)	5.24 (7.92)	269
$\{[Cd_2(btec)(phen)_2(H_2O)_4].H_2O\}_n$	**8**	White	28	42.94 (44.13)	3.32 (3.05)	5.43 (6.05)	>360
$\{[Cd_2(btec)(2,2'\text{-bipy})_2(H_2O)_4].H_2O\}_n$	**9**	White	37	41.79 (41.07)	2.63 (3.21)	5.43 (6.38)	>360
$\{[(UO_2)_2(btec)(phen)_2].4H_2O\}_n$	**10**	Yellow	56	32.51 (33.40)	2.19 (2.14)	3.69 (4.58)	>360
$\{[(UO_2)_2(btec)(2,2'\text{-bipy})_2].2H_2O\}_n$	**11**	Yellow	46	33.70 (31.59)	2.40 (2.20)	4.90 (4.91)	>360

Table 2. IR spectral data of the complexes

Complex		$U_{as(COO)}$	$U_{s(COO)}$	∆U	$U_{(M-N)}$	$U_{(M-O)}$	UH_2O coord-	UH_2O Latttice
$\{[Mn_2(btec)(phen)_2(H_2O)_2].H_2O\}_n$	**1**	1565	1370	195	475	440	3050	3400
$\{[Fe_2(btec)(H_2btec)(phen)_2(H_2O)_2].4H_2O\}_n$	**2**	1580	1380	200	470	438	2900	3430
$\{[Fe_2(btec)(H_2btec)(2,2'\text{-bipy})_2(H_2O)_2].8H_2O\}_n$	**3**	1580	1380	200	460	418	2800	3450
$\{[Co_2(btec)(phen)_2(H_2O)_2].8H_2O\}_n$	**4**	1560	1380	180	464	440	2800	3400
$\{[Ni_2(btec)(phen)_2(H_2O)_2].6H_2O\}_n$	**5**	1550	1365	185	455	422	3100	3450
$\{[Cu_2(btec)(phen)_2(H_2O)_2].H_2O\}_n$	**6**	1545	1395	150	458	430	3100	3450
$\{[Cu_2(btec)(2,2'\text{-bipy})_2].H_2O\}_n$	**7**	1570	1415	155	470	430	2800	3500
{[Cd2(btec)(phen)2(H2O)4].H2O}n	**8**	1570	1375	195	483	442	3050	3300
$\{[Cd_2(btec)(2,2'\text{-bipy})_2(H_2O)_4].H_2O\}_n$	**9**	1560	1375	185	475	435	2800	3450
$\{[(UO_2)_2(btec)(phen)_2].4H_2O\}_n$	**10**	1580	1370	210	490	438	-	3450
$\{[(UO_2)_2(btec)(2,2'\text{-bipy})_2].2H_2O\}_n$	**11**	1585	1370	215	490	438	-	3500

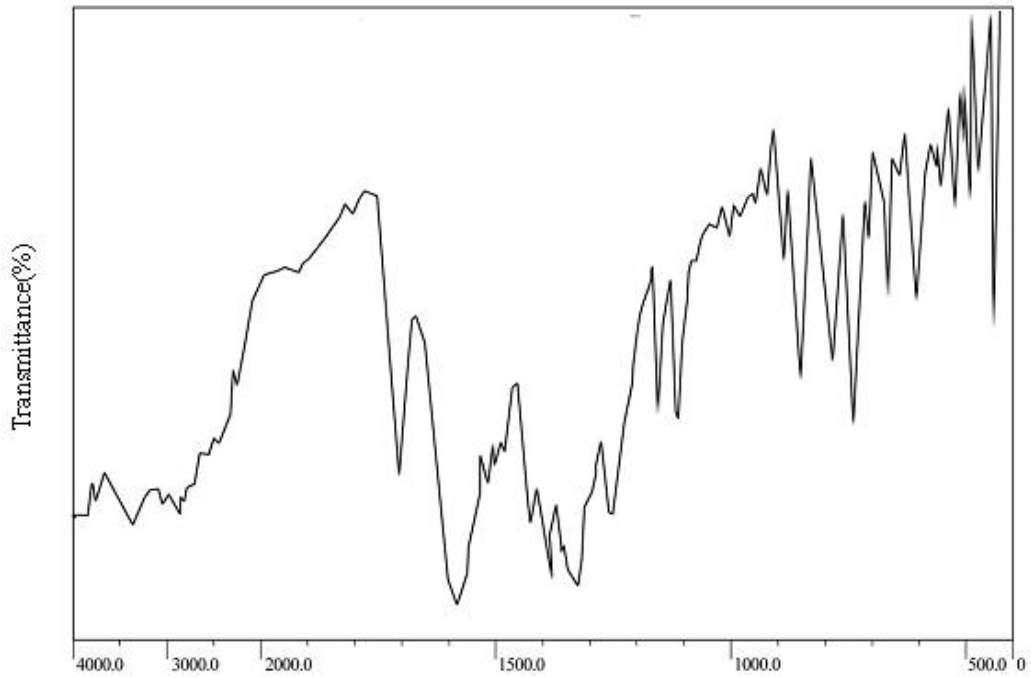

Fig. 2. IR spectrum of{[Fe_2(btec)(H_2btec)(phen)$_2$(H2O)$_2$].4H_2O}$_n$

molecules are located in the range 2800-3100 cm^{-1} [11]. Metal-nitrogen and metal-oxygen bonding are manifested by the appearance of two bands in the 455-490 and 418-442 cm^{-1}regions, respectively [11]. The v(U=O) vibration in the uranyl complexes **10** and **11** are observed as expected as a medium strong band at 900 and 920 cm^{-1}, respectively. They are in a good agreement with those known formany dioxouranium (VI) complexes [12,13].

The IR spectra of the all the prepared complexes show characteristic vibrations of the aromatic nucleus [v(C=C), v(C=N)] for 1,10-phenanthroline and 2,2'-bipyridyl complexes near 700-900, 1420-1490 and 1610-1680 cm^{-1} [14].

3.2 UV-Vis Spectra and Magnetic Susceptibility Measurement

The electronic spectral data of the complexes have been recorded in DMSO. The results are shown in Table 3. The electronic spectra of the complexes present two absorption maxima located in the regions 39,215-35,714 and 35,714-31,250 cm^{-1} due to π→π* and the n→π* transitions within the organic ligands. The band observed in the region 27,777-20,408 cm^{-1} is correlated with an intra ligand charge transfer (IL-charge transfer).

The electronic spectrum of the Mn(**II**) complex **1** is being due to a d^5 ion and therefore it does not show any d-d transitions and no transfer of electrons from the metal to the ligand can occur as well [15]. The complex is probably tetrahedral in structure.

For the two iron(**III**) complexes **2** and **3** the electronic spectra exhibit a band at 19,230 and 18,691 cm^{-1}, respectively, which may be attributed to the transition $^6A_1g \leftarrow {}^2T_2g$, reflecting the octahedral arrangement around the Fe(**III**) [16-18]. The values of their magnetic moments of 3.02 and 3.16 B.M, respectively show an intermediate spin state ($^2T_2$ and $^6A_1$), which means that the Fe(**III**) ion in the complexes exhibits an equilibrium between low and high spin states [19-21].

The cobalt(**II**) coordination polymer **4** displays a magnetic moment values of 4.06 B.M, consistent with an octahedral environment around Co(**II**) [5b,22]. Correspondingly a band appears at 15,748 cm^{-1}, which can be attributed to the transition $^4T_{1g} \leftarrow {}^4A_{2g}$.

The spectrum of the nickel(**II**) complex **5** displays a band at 15,037cm^{-1} assigned to the transition $^3A_2g \leftarrow {}^3T_1g$ [23,24]. The octahedral geometry around the Ni(**II**) ion in this complex is

in agreement with its magnetic moment value of 2.56 B.M.

In case of the two copper(**II**) coordination polymers **6** and **7** only one broad band appears at 16,333 and 17,356 cm^{-1}, respectively, assigned to the $^2B_{1g}\leftarrow{}^2E_{1g}$ transition [25], indicating the octahedral geometry around Cu(**II**). This is supported by their magnetic moment values of 1.10 and 1.09 B.M, respectively. These low values may suggest a binuclear structure for the two Cu(II) complexes.

The electronic spectra of the UO_2(**II**) complexes **10** and **11** exhibit the f-f transition around 12,000 $cm^{-}1$. A band appears at 27,027 and 27,397 cm^{-1}, respectively is assigned to a charge transfer (IL-charge transfer) transition. Furthermore, two bands were recorded in the range 32,000-39,215 correspond to the n→π* and π→π* transitions. A six coordination is assumed around UO_2(**II**) ion [26]. The suggested structures for the ternary complexes are shown in Figs. 3-5.

Table 3. Electronic spectral data of the complexes

Complex		ν_{max} (cm^{-1})	Assignment	μ_{eff} (B.M)
$\{[Mn_2(btec)(phen)_2(H_2O)_2].H_2O\}_n$	**1**	31,746	n→π*	-
		39,215	π → π*	
$\{[Fe_2(btec)(H_2btec)(phen)_2(H_2O)_2].4H_2O\}_n$	**2**	19,230	$^6A_1g\leftarrow{}^2T_2g$	3.02
		25,000	IL-charge transfer	
		32,258	n →π*	
		39,215	π →π*	
$\{[Fe_2(btec)(H_2btec)(2,2'\text{-bipy})_2(H_2O)_2].8H_2O\}_n$	**3**	18,691	$^6A_1g\leftarrow{}^2T_2g$	3.16
		20,408	IL-charge transfer	
		34,482	n →π*	
		38,461	π →π*	
$\{[Co_2(btec)(phen)_2(H_2O)_2].8H_2O\}_n$	**4**	15,748	$^4T_{1g}\leftarrow{}^4A_{2g}$	4.06
		26,315	IL-charge transfer	
		35,714	n →π*	
		38,461	π →π*	
$\{[Ni_2(btec)(phen)_2(H_2O)_2].6H_2O\}_n$	**5**	15,037	$^3A_2g\leftarrow{}^3T_1g$	2.56
		35,714	n→π*	
		38,461	π →π	
$\{[Cu_2(btec)(phen)_2(H_2O)_2].H_2O\}_n$	**6**	16,333	$^2B_{1g}\leftarrow{}^2E_{1g}$	1.10
		26,666	IL-charge transfer	
		34,482	n→π*	
		36,363	π →π*	
$\{[Cu_2(btec)(2,2'\text{-bipy})_2].H_2O\}_n$	**7**	17,356	$^2B_{1g}\leftarrow{}^2E_{1g}$	1.09
		27,777	IL-charge transfer	
		34,482	n →π*	
		38,461	π →π*	
$\{[Cd_2(btec)(phen)_2(H_2O)_4].H_2O\}_n$	**8**	33,333	n →π*	-
		38,461	π →π*	
$\{[Cd_2(btec)(2,2'\text{-bipy})_2(H_2O)_4].H_2O\}_n$	**9**	33333	n →π*	-
		38,461	π→π*	
$\{[(UO_2)_2(btec)(phen)_2].4H_2O\}_n$	**10**	12,820	f-f transition	-
		27,027	IL-charge transfer	
		32,000	n →π*	
		39,215	π →π*	
$\{[(UO_2)_2(btec)(2,2'\text{-bipy})_2].2H_2O\}_n$	**11**	12,987	f-f transition	-
		27,397	IL-charge transfer	
		33333	n →π*	
		39,215	π →π*	

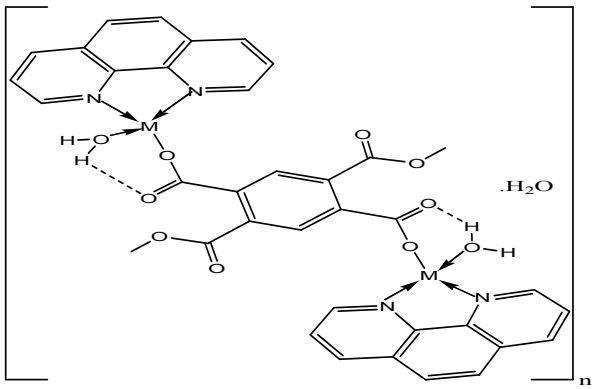

Fig. 3. Suggested structure of $\{[M_{n2}(btec)(phen)_2(H_2O)_2].H_2O\}_n$
M= Mn(II) or Cu(II)
(Complexes 1, 6)

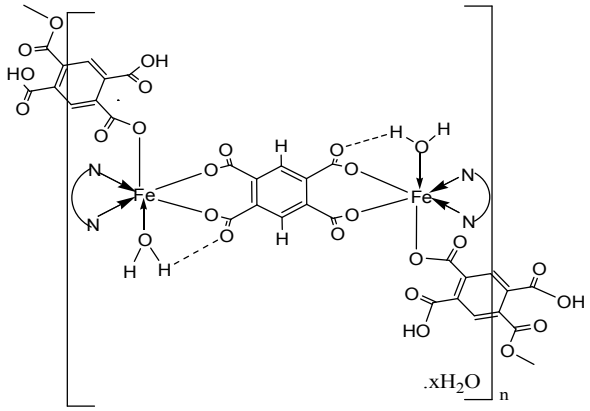

Fig. 4. Suggested structure of $\{[Fe_2(btec)(H_2btec)(diamine)_2(H_2O)_2].xH_2O\}_n$
wherediamine=1,10-phenanthroline or 2,2-bipyridin (N-N), x= 4 or 8
(Complexes 2, 3)

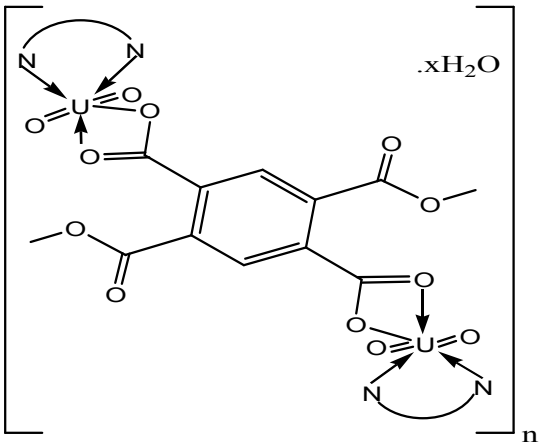

Fig. 5. Suggested structure of$\{[(UO_2)_2(btec)(N\text{-}N)_2].xH_2O\}_n$
where x= 4 or 2.
(Complexes 10, 11)

3.3 Thermal Decomposition of the Complexes in Dynamic Air

Two illustrative examples for the thermal decomposition of the complexes are described as follows. The thermal data of the complexes are listed in Table 4.

The TGA curve of $\{[Mn_2(btec)(phen)_2(H_2O)_2].H_2O\}_n$ exhibits three mass loss stages (Fig.6). The first mass loss occurs in the range 118–151ºC corresponding to the loss of a lattice water molecule (calc. 2.3%, found 2.1 %). For this step the DTG curve shows a peak at 131ºC and an endothermic DTA peak at 135ºC was recorded. The second step at 152-193ºC is associated with the loss of the two coordinated water molecules (calc. 4.6%, found 4.1%). The mass loss in percent, due to the release of lattice and coordinated water molecules as calculated from the TG curve, is in agreement with the elemental analysis results within ±3%. After that a plateau extends from 220 to 352°C indicating the stability of the anhydrous compound up to 352ºC. A DTG midpoint at 166°C and an endothermic effect at 169ºC in the DTA curve were recorded. The third step at 400-459ºC is assigned to decomposition of the two phen and $btec^{-4}$ ligands (calc. 78.8%, found 75.8%). A DTG peak shows this thermal event at 423ºC and an exothermic DTA peak occurs at 444ºC. The mass left after the final decomposition is in agreement with the formation of Mn_2O_3 (calc. 20.3 %, found 19.0 %).

The pyrolysis TG curve (Fig.7) of $\{[Cu_2(btec)(phen)_2(H_2O)_2].H_2O\}$ is characterized by three steps in the temperature ranges at 65-118, 120- 180 and 196-479ºC. The first mass loss is commensurate with the expulsion of the lattice water molecule (calc. 2.2%, found 2.5%). The DTG curve shows a peak at 93ºC and the DTA curve gives an endothermic peak at 91ºC. The second step mass loss is related to the loss of the two coordinated water molecules (calc. 4.5%, found 4.0%). For this step a DTG peak at 145ºC and an endothermic peak in the DTA curve at 147ºC are observed. The third stage is composed of overlapping steps and shows a mass loss indicating decomposition of two phen and a $btec^{-4}$ ligands (calc. 77.0%, found 75.4%). This step is marked on the DTG curve as three peaks at 223, 257 and 450ºC with associated exothermic peaks in the DTA curve at 229, 266 and 452ºC. The final product indicates that the residue is2CuO (calc. 19.1%, found 18.1%).

3.4 A Comment

Comparing the TG curves of the above two complexes one can observe that the two complexes are of the same composition but differ in the coordinated metal ion. It is clear from the initial decomposition of the three steps in each of the two TG curves that the copper(II) complex steps occur at lower temperatures than those of the manganese (II) complex, indicating the autocatalytic effect of the Cu(II) on the decomposition of its complex.

3.5 Kinetic Analysis Parameters

The kineticparameters such as activation energy (**E***) and pre-exponential factor (**Z**) and order of the decomposition reactions were evaluated graphically by employing the Coats–Redfern [27] (equations 6 & 7).

The Coats-Redfern equation:

$$\ln[1-(1-\alpha)^{1-n}/(1-n)T^2] = M/T + B \quad \text{for } n \neq 1 \qquad (6)$$

$$\ln[-\ln(1-\alpha)/T^2] = M/T + B \quad \text{for } n = 1 \qquad (7)$$

where **α** is the fraction of material decomposed, **n** is the order of the decomposition reaction and M=E/R and B=ZR/ΦE*; **E***, **R**, **Z** and **Φ** are the activation energy, gas constant, pre-exponential factor and heating rate, respectively.

The correlation coefficient ***r***is computed using the least squares method for equations (6) and (7). Linear curves were drawn for different values of **n** ranging from 0 to 2. The value of **n**, which gave the best fit, was chosen as the order parameter for the decomposition stage of interest. The kinetic parameters were calculated from the plots of the left hand side of equations (6), (7), against 1/T.

The thermodynamic parameters Δ**S***(J $K^{-1}mol^{-1}$), Δ**H***($kJmol^{-1}$) and Δ**G***($kJmol^{-1}$) were calculated using the following equations:

$$\Delta S^* = 2.303R \log (Zh/kT) \qquad (8)$$

$$\Delta H^* = E^* - RT \qquad (9)$$

$$\Delta G^* = \Delta H^* - T\Delta S \qquad (10)$$

Where **Z**, **k**, and **h** are the pre-exponential factor, Boltzmann, and Plank constants, respectively. The kinetic and thermodynamic parameters of compounds **1** and **4** are summarized in Table 5.

Table 4. Thermal decomposition data of the complexes in dynamic air

Complex		Step	TG/DTG			Mass loss (%)
			Ti/ºC	Tm/ºC	Tf/ºC	
$\{[Mn_2(btec)(phen)_2(H_2O)_2].H_2O\}_n$	**1**	1st	118	131	151	2.1
		2nd	152	166	193	4.1
		3rd	400	423	459	75.8
$\{[Fe_2(btec)(H_2btec)(phen)_2(H_2O)_2].4H_2O\}_n$	**2**	1st	24	61	94	6.1
		2nd	96	234	241	3.3
		3rd	242	359	434	76.5
$\{[Co_2(btec)(phen)_2(H_2O)_2].8H_2O\}_n$	**4**	1st	61	108	112	8.00
		2nd	113	119	147	10.0
		3rd	336	389	434	64.6
$\{[Ni_2(btec)(phen)_2(H_2O)_2].6H_2O\}_n$	**5**	1st	65	107	123	3.00
		2nd	124	148	164	11.0
		3rd	180	410	455	69.6
$\{[Cu_2(btec)(phen)_2(H_2O)_2].H_2O\}_n$	**6**	1st	65	93	118	2.50
		2nd	120	145	180	4.00
		3rd	196	257	479	75.4
$\{[Cu_2(btec)(2,2\text{-bipy})_2].H_2O\}_n$	**7**	1st	47	70	131	2.30
		2nd	132	271	311	44.7
		3rd	312	418	459	33.0
$\{[Cd_2(btec)(phen)_2(H_2O)_4].H_2O\}_n$	**8**	1st	30	51	83	1.2
		2nd	137	148	192	6.0
		3rd	193	456	380	64.5
$\{[Cd_2(btec)(2,2\text{-bipy})_2(H_2O)_4].H_2O\}_n$	**9**	1st	75	95	124	2.1
		2nd	125	143	160	7.5
		3rd	290	369	523	60.4
$\{[(UO_2)_2(btec)(phen)_2].4H_2O\}_n$	**10**	1st	50	57	74	6.0
		2nd	395	477	492	45.9
$\{[(UO_2)_2(btec)(2,2\text{-bipy})_2].2H_2O\}_n$	**11**	1st	25	76	114	3.7
		2nd	374	436	463	46.6

T_i=Initial temperature & T_m=Maximum temperature & T_f=Final temperature

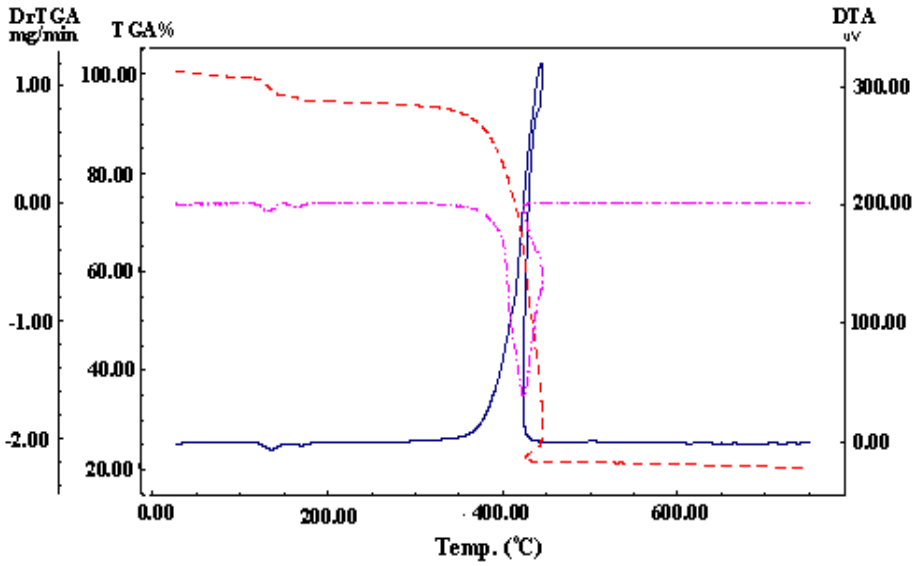

Fig. 6. TG-DTG-DTA curves of $[Mn_2(btec)(phen)_2(H_2O)_2]_nH_2O$

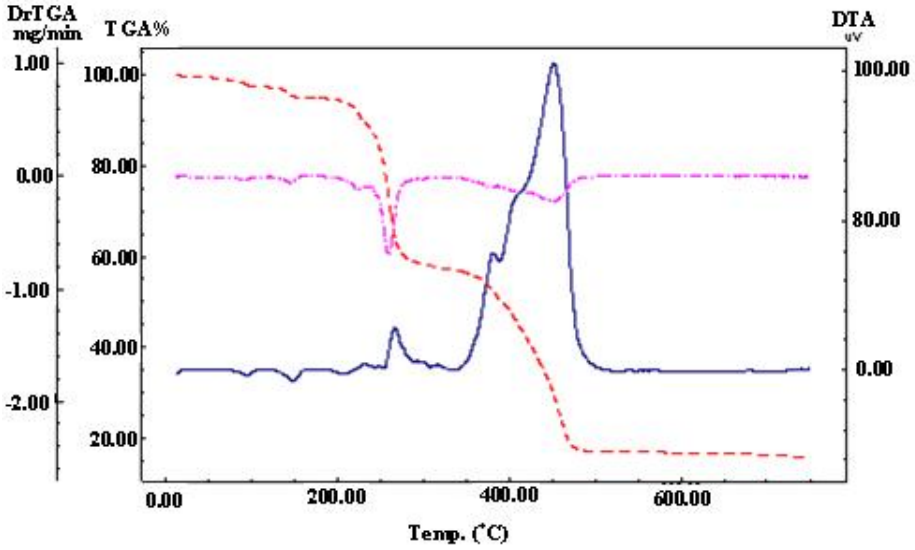

Fig. 7. TG-DTG-DTA curves of $\{[Cu_2(btec)(phen)_2(H_2O)_2].H_2O\}_n$

Table 5. Kinetic and thermodynamic parameters of the complexes 1 and 6 in dynamic air

Complex	Step	*r*	n	E*	Z	ΔH*	ΔS*	ΔG*
1	**1st**	0.9824	0.00	70.09	3.2×10^{8}	66.67	-0.22712	160.24
		0.9897	0.33	84.81	4.5×10^{10}	81.39	-0.26251	189.54
		0.9926	0.50	93.37	3.8×10^{10}	89.95	-0.28318	206.62
		0.9948	0.66	102.1	2.9×10^{12}	98.65	-0.30423	223.99
		0.9981	1.00	122.6	7.3×10^{18}	119.26	-0.35427	265.22
		0.9995	2.00	199.9	9.9×10^{24}	196.5	-0.5431	420.32
4	**1st**	0.9867	0.00	35.80	1.6×10^{5}	32.54	-0.15611	93.94
		0.9974	0.33	52.02	1.3×10^{6}	48.75	-0.19603	125.85
		0.9996	0.50	62.71	5.2×10^{8}	59.44	-0.22271	147.03
		0.9999	0.66	74.46	1.5×10^{11}	71.19	-0.25224	170.41
		0.9969	1.00	105.5	1.2×10^{15}	102.24	-0.33086	232.38
		0.9805	2.00	243.8	3.5×10^{33}	240.58	-0.68545	510.19

Order (n), Z (s^{-1}), E(kJ mol^{-1}), Δ H*(kJ mol^{-1}), ΔS*(JK^{-1} mol^{-1}), ΔG*(kJ mol^{-1})*

3.6 X-ray Powder Diffraction

The X–ray powder diffraction patterns of the six complexes **2**, **5**, **7**, **9** and **11** were recorded. The crystal lattice parameters were computed with the aid of the computer program TREOR. The observed 2Θ with relative intensity more than 10 % are indexed and have been used for evaluation. The crystal data of all the complexes fit well with the triclinic crystal system (Table 6). The crystal lattice parameters show variations in their values with the coordinated metal ions of different sizes indicating the effect of the metal nature on the metal- oxygen or metal-nitrogen bond strength. These parameters point also to the distorted octahedral environment around the metal ions in the complexes.

3.7 Nano-sized Metal Coordination Polymers

The average particle size could be calculated from the powder X-ray diffraction of the above complexes and by application of the Scherrer` sequation:

$$D = 0.94\lambda / \beta \cos\theta \qquad (11)$$

Where **λ** is the wavelength of the X-ray used, **β** is the Full Width at Half Maximum (FWHM), **D** is the particle size and **θ** is the angle between the incident and the scattered X-ray. Table 7 includes the average particle size of the complexes. X-ray powder diffraction pattern of compound **7** is illustrated in Fig. 8.

Table 6. The crystal data of the complexes

Complex	2	5	7	9	11
***a*(Å)**	5.824	8.557	5.859	10.589	5.641
***b*(Å)**	8.528	8.851	10.824	9.609	10.027
***c*(Å)**	24.837	13.851	11.494	12.423	8.418
***α*(d)**	59.842	80.521	91.516	94.269	92.161
***β*(d)**	69.217	86.106	95.620	120.71	73.789
***γ*(d)**	61.563	86.547	95.781	67.13	135.91
Volume unit cell ($Å^3$)	989.38	1000	721.40	998.40	308.59
Crystal system	Triclinic	Triclinic	Triclinic	Triclinic	Triclinic

Table 7. The average particle size of the complexes (nm)

Complex	2	5	7	9	11
Average particle size	6.4	19.4	25.4	12.6	13.5

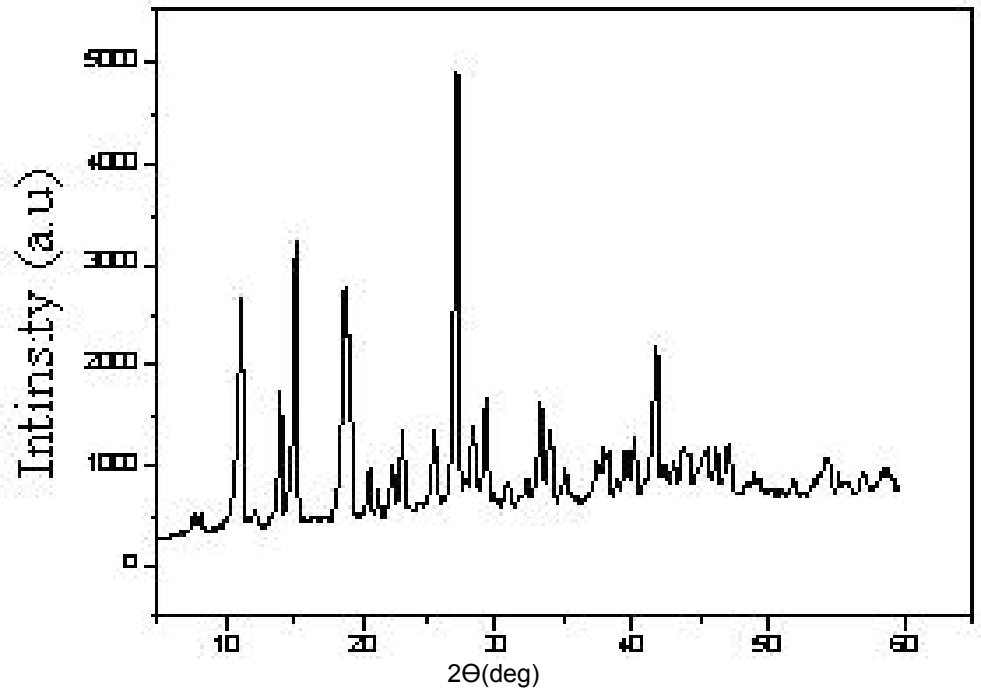

Fig. 8. X-ray powder diffraction pattern of complex 7

3.8 Microbiological Screening

The following bacterial and fungal strains were used to test the antimicrobial activity of compounds **6** and **7**: *Bacillus cereus* (G^{+ve}), *Staphylococcus aureus* (G^{+ve}), *Escherichia coli* (G^{-ve}), *Pseudomonas aeruginosa* (G^{-ve}), *Serratia marescens* (G^{-ve}), *Aspergillus flavus*, Candida *albicans*, Fusarium *oxysporum*, *Geotrichum candidum*, *Scopulariopsis brevicaulis*, *Trichophton rubrum*. The screening revealed that compounds **6** and **7** exhibit only high antibacterial activity against both *Escherichia coli* (-ve*)* and *Bacillus cereus* (+ve), otherwise the two compounds display no noticeable activity (Table 8). It is to be noted that these two complexes are complexes of Cu(II) which is known for its antimicrobial activity. According to the chelation theory, chelation of Cu(II) to btec and phen or 2, 2`-bipy enhances its activity. That these two compounds are active may be attributed to their better lipophilicity than the other compounds and consequently the ability to penetrate the cell membrane.

Table 8. Antimicrobial activity of the complexes (inhibition zones in cm)

Samples no / Organisms	6	7
Serratia marescens (-ve)	0	0
Pseudomonas aeruginosa (-ve)	0	0
Escherichia coli (-ve)	12	22
Staphylococcus aureus (+ve)	0	0
Bacillus cereus(+ve)	16	18
Samples no / Organisms	**6**	**7**
Candida albicans	0	0
Geotrichum candidum	0	0
Fusarium oxysporum	0	0
Scopulariopsis brevicaulis	0	0
Trichophton rubrum	0	0
Aspergillus flavus	0	0

where S.M=Serratia marcescens, E.C=Escherichia coli, S.A= Staphylococcus aureus, B.C = Bacillus cereus.

4. CONCLUSION

The above mentioned mixed ligand coordination polymers were prepared by a procedure which is different from those reported in the literature, thus leading to isolation of compounds of variable contents of coordinated and crystal water. Moreover, in this article investigated thermal behavior, particle size calculation and biological screening (not reported in the literature) provide new properties of these coordination polymers. The structural aspects which can be concluded from this work involve the existence of two types of coordinated carboxylates in the iron(III) complexes and in the same molecule one is abidentate and the other is a bridging monodentate. For the Mn(II), Co(II), Ni(II), Cu(II) and Cd(II) complexes, the carboxylate is a bridging monodentate, while for the uranyl complexes it is a bidentate.

ACKNOWLEDGEMENTS

One of the authors (A. A. M. Aly) is very grateful To the Alexander von Humboldt Foundation, Germany, for donating the magnetic susceptibility balance (MSB-Auto).

COMPETING INTERESTS

Authors have declared that no competing interests exist.

REFERENCES

1. Goldworthy JS, Pochodylo AL, LaDuca RL. Manganese and cobalt *para*-benzenedicarboxylate coordination polymers with 3-pyridylisonicotinamidecoligands: Different layer topologies and a self-penetrated supra molecular network. Inorg. Chim. Acta 2014; 419: 26b)O`Keefe M, Yaghi OM. Deconstructing the crystal structures of metal-organic frameworks and related materials into their underlying nets. Chem. Rev. 2012;112:675 .

2. a) Barton TJ, Bull LM, Klemperer WG, Loy DA, McEnaney B, Misono M, Monson PA, Pez G, SchererGW,Vartuli JC, Yaghi OM. Tailored porous materials. Chem. Mater. 1999;11:2633. b) Geng JC, Liu LW, Xiao SL, Cui GH. Two 2D cobalt (II) coordination frameworks with unusual binodal network topology: synthesis, structures, and catalytic properties. Transition Met. Chem. 2013; 38:143 c) Henkelis JJ, Barnett SA, Harding LP, Hardie MJ. Coordination polymersutilizing *N*-oxide functionalized host ligands. Inorg. Chem. 2012;51:10657

3. a) Xiao SL, Liu YG, Ma PJ. Effect of carboxylate coligands on the crystal structures of two nickel(II) coordination polymers constructed from a flexiblebis(5,6-dimethylbenzimidazole) ligand. Transition Met. Chem. 2013; 38:793. b) Wang XL, Gao Q, Tian AX, Liu GC. Inserting -$(CH_2)_n$- (*n* = 2, 3, 4) spacers into the reactant mercapto-methyltetrazole ligand for tuning the multinuclear Ag(I) clustersin Keggin-based compounds. Cryst. Growth Des. 2012;12:2346. c) Mori W, Inoue F, Yoshida K, Nakayama H, Takamizawa S, Kishita M. Synthesis of new adsorbent copper(II)terephthalate. Chem. Lett. 1997;12:1219.

4. a) Xiao SL, Li GY, Qin L, Gui GH. The role of Ag…O and Ag…Ag interactions in silver(I) supra molecular frameworks constructed from benzene multicarboxylate and nitrogen ligands. Transition Met. Chem., 2013; 38:779 b) Shao KZ, Zhao YH, Lan YQ, Wang XL, Su ZM, Wang RS.Molecular tectonics of metal–organic frameworks based on ligand-modulated polynuclear zinc SBUs and aromaticmulticarboxylic acids. Cryst Eng Comm. 2011;13:889.

5. a) Yanjuan Q, Hui L, Feijun G, Minhua C. Changwen H.A two-dimensionalstrong hydrogen-bond network constructed from a transition metal with apolycarboxylato ligand. J. Coord. Chem. 2006;59:505(2006). b) Yanfei Q, Xinlong W, Enbo W, Chao Q, Hao N. Two new metalcoordination polymers containing mixed ligands: hydrothermalsynthesis and crystal structures of $[Co_2(1,2,4,5\text{-btc})(phen)_2(H_2O)_6]\cdot 2H_2O$ and $[Mn_3(1,2,4\text{-btc})_2(phen)_2(H_2O)_2]_n$. J. Coord. Chem. 2005; 58:1289. c)Ji-xin Y, Mao-lin H, Ju-xia L, Xin-yuan S. Chem. Res. Chin. Un. 2005;21:21.
6. Liu D, Kwasniewska K. An improved agar plate method for rapid assessment of chemical inhibition to microbial populations. Bull. Environ. Contam. Toxicol. 1981;27:289.
7. Nakamoto K. Infrared and Raman Spectra of Inorganic and Coordination Compounds, 3rd ed., Wiley, New York; 1978.
8. Wang YY, Shi Q, Shi QZ, Gao YC, Zhou ZY. Syntheses, characterization and crystal structure of copper(II) α,β-unsaturated carboxylate complexes with imidazole. Polyhedron. 1999;18:2009.
9. Brzyska W, Kowalewicz J, Zesz. Nauk. Politech. Slask. Chem. 1981;677:141.
10. Bravo A, Anacona JR. Metal complexes of the flavonoid quercetin: antibacterial properties. Transition Met. Chem. 2001;26:20.
11. Rakha TH. Transition metal chelates derived from potassium nicotinoyldithiocarbazate (KHNDC). Synth. React. Inorg. Met.-Org. Chem. 2000;30:205.
12. McGlynm SP, Smish JK, Neely WC. Electronic structure, spectra, andmagneticpropertiesofoxycations.III. Ligation effects on the infrared spectrum of the uranyIIon. J. Chem. Phys. 1961;35:105.
13. Jones LH. Determination of UO bond distance in uranyl complexes from the irinfrared spectra. Spectrochim. Acta. 1959;15:409.
14. Ali MA DA. Chowdhury DA, Vddin MN. Four-and five-coordinate copper (II) complexes containing mixed ligands. Polyhedron. 1984;3:595.
15. Shrivastava VS, Bhasin CP, Saxena GC. Spectral, magnetic and antibacterial studies of some newly synthesized manganese (II),cobalt (II),nickel (II) and copper (II)complexes. J. Indian Chem. Soc. 1986;63:865.
16. Scarpellini M, Neves A, Bortoluzzi AJ, Vencato I, Drago V, Ortiz WA, Zucco C. Anew $Fe^{III}(\mu\text{-}OCH_3)_2(\mu\text{-}OAc)Fe^{III}$ complex containing phenolate and imidazole ligands as a structural model for the active site of non-heme diiron enzymes. J. Chem. Soc. Dalton Trans. 2001;2616.
17. Westerheide L, Muller FK, Than R, Krebs B, Dietrich J, Schindler S. Syntheses and structural characterization of dinuclear and tetranucleariron(III) complexes with dinucleating ligands and the irreactions with hydrogenperoxide. Inorg. Chem. 2001;40:1951.
18. Rowland JM, Olmstead M, Mascharak PK. Syntheses, structures, and reactivity of low spiniron(III)complexes containing as ingle carboxamido nitrogenin a$[FeN_5L]$ chromophore. Inorg. Chem. 2001;40:2810.
19. Martin RT, White AH, Trans. Metal Chem. 1968;4:113.
20. JØrgensen CK. Absorption spectra of transition group complexes of sulphur-containing ligands. J. inorg. Nuclear Chem. 1962;24:1571.
21. Ewald AH, Martin RL, Sinn E , White AH. Electronic equilibrium between the $^6A_1$ and $^2T_2$ states iniron(III)dithiochelates. Inorg. Chem. 1969;8:1837.
22. Lopez-Gresa MP, Ortiz R, Perello L, Latorre J, Liu-Gonzalez M, Garcıa-Granda S, Perez-Priede M, Canton E. Interactions of metal ions with two quinolone antimicrobial agents(cinoxacin and ciprofloxacin):spectroscopic andX-ray structural characterization. Antibacterial studies. J. Inorg. Biochem. 2002;92:65.
23. Singh B, Srivastava U. Studies on methyl N-(2-thiazolyl) dithiocarbamate complexes of some bivalent-metal ions.Indian J. Chem. 1989;28:431.
24. Mendoza-Díaz G, Ireta-Moreno J. Synthesis and characterization of zinc mixed complexes with nalidixate anion and (N-N) donors. J. Inorg. Biochem.1994;54: 235 .

25. Raman N, Raja JD, Sakthivel A. Design, synthesis, spectroscopic characterization, biological screening, and DNA nuclease activity of transition metal complexes derived from a tridentate Schiff base. Russ. J. Coord. Chem. 2008;34:400.

26. Jiang Y, Yu Z, Liao Z, Li G, Chen J. Syntheses and photo luminescent properties of two uranyl-containing compounds with extended structures. Polyhedron. 2006;25:1359.

27. Coats AW, Redfern JP. Kinetic parameters from thermogravimetric data. Nature. 1964;201:68.

Peer-review history:
The peer review history for this paper can be accessed here:
http://www.sciencedomain.org/review-history.php?iid=901&id=16&aid=8348